RESEARCH ARTICLE OPEN ACCESS

Design and Analysis of a Hybrid VTOL UAV for Medical Cargo Delivery

AVN Ravi[1], Kiran Kumar[2], Nikhil S N[3], Ronith P[4], Prathik S Jain[5], Shuja Khan[6], Sahevaan Taneja[7]
1-4 Student, Aeronautical Engineering, Dayananda Sagar College of Engineering, Bangalore
Email: kirankumarstumbagi@gmail.com
5 Assistant Professor, Aeronautical Engineering, Dayananda Sagar College of Engineering, Bangalore
Email: prathiks-ae@dayanandasagar.edu
6 UAV, T-Works, Hyderabad
Email : shuja@tworks.in
7 UAV, T-Works, Hyderabad
Email: sahevaantaneja@gmail.com

Abstract:

Unmanned aircraft systems are extensively used by the military. The use of remotely piloted aircraft systems (RPAS) and small drones has expanded to perform civilian tasks such as search & rescue operations, delivering goods, aerial cinematography & to spray pesticides and track crop growth patterns in agriculture. Healthcare is the foremost requirement for the citizens of a country. However, unfortunately medical services in rural areas of several countries including India lag considerably. Providing quality healthcare to rural populations is vital, but is a highly overlooked issue in the developing world. With more than 70% of the country's population living in rural areas, the lack of access to these basic facilities has proven to be disastrous. One of the most valued areas of drone development in healthcare industries is to deliver medicines, vaccines, blood, and other medical supplies.

This paper presents a solution proposed by employing an Unmanned Aerial Vehicle (UAV) for medical supply delivery in remote areas inaccessible by road. The UAV developed is a 2500mm wingspan hybrid VTOL with a payload capacity of about 1000g. It is capable of vertical take off and landing making it optimal for operating in rural areas without sophisticated runways.

Keywords — **Hybrid VTOL, Medical Cargo Delivery, Additive Manufacturing, Modal Analysis, CFD Analysis**

I. INTRODUCTION

An Unmanned Aerial Vehicle (UAV) is an aerial vehicle which has no human pilot on board. It can be controlled from ground or be autonomously controlled with a computer on board. UAVs have found their application in the fields of defence, transport, agriculture and recreation, to name a few. In recent decades, with rapid development, UAVs have become an integral part of global aerospace industry. Doctors began testing the transport of diagnostic samples between remote and central testing facilities during a tuberculosis outbreak in Papua New Guinea as early as 2014. As other countries witnessed the possibilities, the first big leap forward took place in Rwanda, where experiments matured into national scale delivering blood on-demand and at scheduled intervals.

The aircraft is designed and manufactured to address challenges of rural access to medical supplies. This aircraft is VTOL capable making it optimal in operating in areas without a sophisticated runway. Electric propulsion by Brushless DC (BLDC) motors is employed for vertical take-off and landings whereas forward flight constitutes majority of the flight time and hence an IC engine is used. Hence, the term Hybrid VTOL aircraft.

In this paper, we model, design and analyse a Hybrid VTOL to deliver medical Cargo of 1000 grams with an endurance of 60 minutes. The design will also consist of fully autonomous take-off and landing along with telemetry data collection.

II. METHODOLOGY – CONFIGURATION SELECTION & DESIGN

Airfoil selection and wing planform selection is done by performing a weighted score method where each type is rated from 1 (least suitable) to 3 (best suitable) against certain parameters.

A. Airfoil Selection

Airfoil selection is done by considering their performance at a Reynolds' number of 500,000. Airfoils are shortlisted based on required C_l for optimum aircraft performance and flat bottom profile. Cambered airofoils are not preferred as they contribute significantly to drag. Selection is carried out considering performance of N-10, CLARK-Y and Drela AG03 as shown in the Table 1.

TABLE 1
AIRFOIL CONFIGURATION SELECTION TABLE

Parameters	Clark Y	DRELA AG03	N-10
Drag Coefficient	1	3	2
C_l/C_d	3	1	2
Manufacturing Complexity	1	2	3
Total	5	6	7

Upon analysing these airfoils on XFLR, it was found that N-10 has higher C_l at normal operating ranges while maintaining low C_d. The stall characteristics is smooth so there is no sudden drop in lift if the wing encounters a stall which gives the pilot extra ease of recoverability and greater control. The stall angle for N-10 is found to be 15.5 degrees.

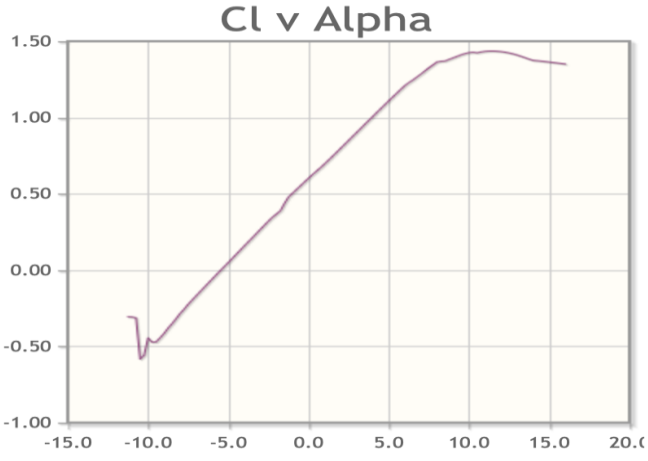

Fig. 1 Cl v Alpha graph

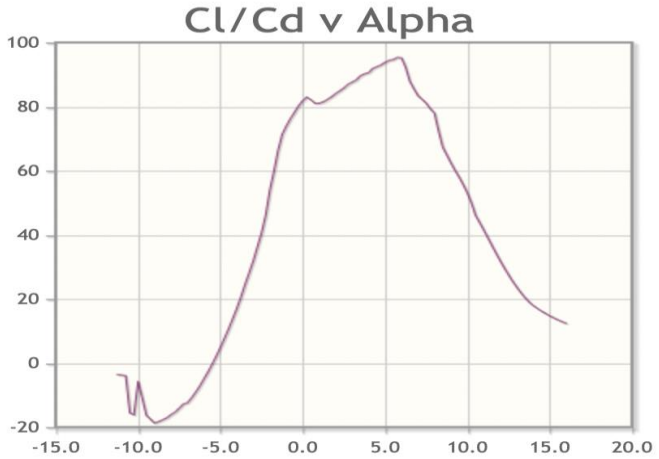

Fig. 2 Cl/Cd v Alpha graph

The highest C_l/C_d for N-10 is found to be at an angle of 5 degrees which helps decide on the wing incidence and placement.

B. Wing Configuration Selection

Rectangular, tapered and elliptical planforms are shortlisted due to prior work experience and familiarity. Table 2 shows selection process based on various parameters.

TABLE 2
WING PLANFORM CONFIGURATION SELECTION TABLE

Parameters	Rectangular	Elliptical	Tapered
Induced Drag	1	3	2
Weight	1	2	3
Tip Stall Characteristics	3	1	2
Manufacturing Complexity	3	1	2
Total	8	7	9

Tapered wing planform is chosen due to lower drag, improved manoeuvrability and relatively simple structure compared to an elliptical planform.

Wing Structure

Wing is manufactured using balsa and aeroply in 3 sections which are integrated into one whole wing by telescopic slide and lock mechanism. Commercially available carbon fiber tubes are used as spars. Ribs of N10 shaped airfoils are placed along the span to define the contour of the wing. 22 ribs are used in total out of which 14 are made of balsa, 8 are made of aeroply as shown in the Fig. 3.

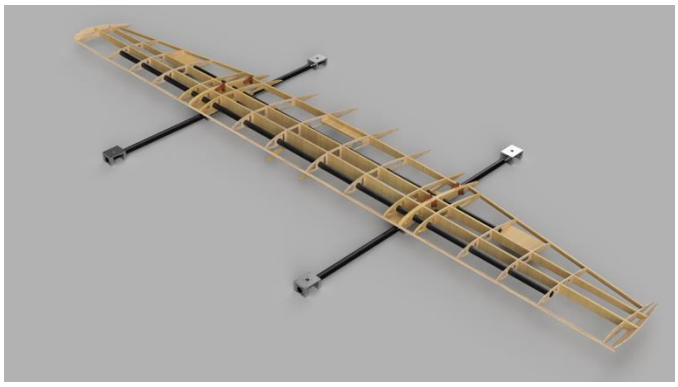

Fig. 3 Wing Structure

Monokote, a synthetic heat activated covering film is covered over the wing structure to enhance torsional rigidity of the wing. Ailerons are placed at the outboard section of the wing and sized to provide effective control over the aircraft. The servos are placed close to and perpendicular to the hinge line to reduce the control rod length, increase the resolution of servo arm movement and prevent control surface warp.

Further, specially designed Aluminium clamps are used to mount the 4 motors onto the CF rods, which extend out of the wing.

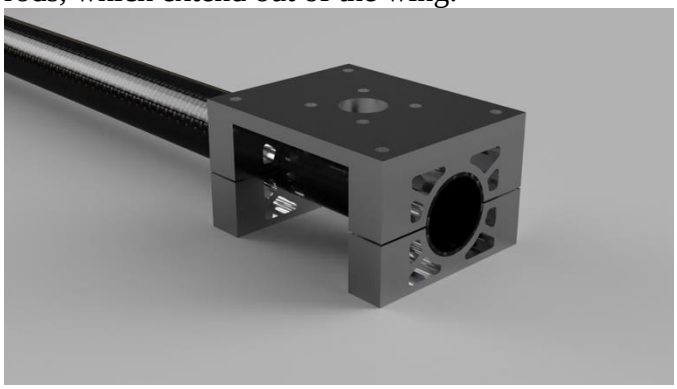

Fig. 4 VTOL Motor Mount

The clamps are designed and manufactured using CNC routing to fit perfectly around the CF rod and consist of the required strength to function as a motor mount.

C. Empennage Configuration Selection

V Tail, T Tail & U Tail were shortlisted based on propeller wake region and empennage weight and are tabulated as shown in Table 3. Empennage configuration is done considering parameters such as weight, wetted area, tail efficiency and manufacturing complexity. The V-Tail has fewer surfaces, has lesser wetted area and thus produces lesser induced and parasitic drag. In most propeller aircrafts, the power plant is usually placed outside the aircraft in front of the nose, in such cases a V-tail is used to avoid placing the vertical stabilizer in propeller wake region, which would disrupt the flow of exhaust, reducing thrust and increasing wear on the stabilizer. The complete tail section is 3D printed using PLA Pro. The V-Tail has a circular chord wise cut section in the centre to accommodate a CF tube. It has two circular span wise holes to accommodate spars for rigidity and special slots to place the servo. The empennage is shown pictorially in Fig. 5.

TABLE 3
EMPENNAGE CONFIGURATION SELECTION TABLE

Parameters	V – Tail	T -Tail	U – Tail
Weight	3	2	1
Wetted – Area	3	1	2
Tail Efficiency	1	3	2
Manufacturing Complexity	2	1	3
Total	9	7	8

Fig. 5 3D Printed V Tail

D. Fuselage Structure

A Semi-Monocoque fuselage is made of aeroply and balsa. Aeroply has high strength and balsa is light in weight, hence together they improve the overall structural strength while maintaining the weight. It comprises 8 formers and 1 motor mount held together by longerons and balsa sheet covering. The structure of the fuselage is shown in Fig. 6 and fuselage with sheet covering is shown in Fig. 7. A compartment with trays is designed in the nose section and rear taper section to carry the propulsion system and communication modules. The dimensions of fuselage are tabulated as shown in Table 4.

Salient features of the fuselage include,

- A dedicated and distinguished cargo and electronics bay
- Reduced frontal area for minimum drag and maximum usage of propeller
- Semi-Monocoque structure for high structural strength and aerodynamic efficiency
- A dedicated attachment for the boom for increased strength and reduced flow separation

TABLE 4
FUSELAGE DIMENSIONS

Parameters	Values
Length	1050mm
Width	200mm
Height	275mm

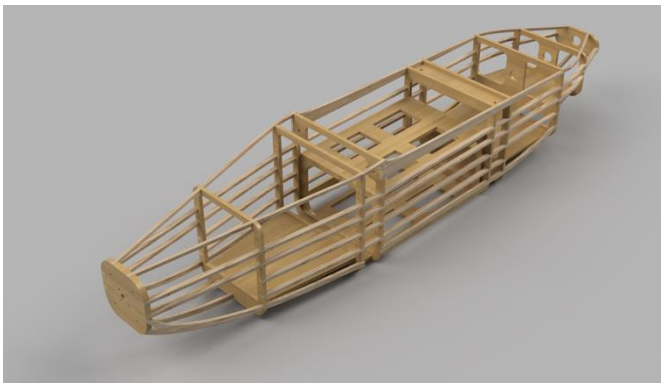

Fig. 6 Fuselage Internal Structure

Fig. 7 Fuselage with Sheet Covering

E. Final Assembly & Airframe Integration

The selected planforms are designed and assembled to obtain the structure as shown in Fig. 8. Further the assembly is subjected to analysis to validate the structural strength and aerodynamic performance.

Fig. 8 Final Assembly

III. STABILITY & CONTROL

The aircraft wing leading edge (LE) is taken as the datum line to calculate CG and the same datum has been used to show the CG location on the wing. The empty and loaded CG of the aircraft co-incide and the required stability margins along with the Neutral Point (NP) and Aerodynamic-Center (AC) distances have been tabulated, as shown below in Table 5.

TABLE 5
STABILITY PARAMETERS

Parameters	Values
Position of NP	135mm from LE
Static Margin	15%
Position of CG	81mm from LE
Position of AC	90mm from LE

Static and dynamic stability derivatives for longitudinal and directional parameters were calculated and are tabulated in Table 6. They were seen to be in the right range validating the plane's static and dynamic stability.

TABLE 6
STABILITY DERIVATIVES TABLE

Stability Parameter	Symbol	Range (per rad)	Effective Value (per rad)
Static Longitudinal Stability	$C_{m\,\alpha}$	-0.3 to -1.5	-0.588
Dynamic	C_{mq}	-5 to -40	-5.350

Longitudinal Stability			
Static Directional Stability	$C_{n\beta}$	+0.05 to +0.4	+0.053
Dynamic Directional Stability	C_{nr}	-0.01 to -1	-0.047

Control surface sizing was done to design suitable primary surfaces which would provide the required 3D control over the plane during flight. The span and mean aerodynamic chord (MAC) of the primary surfaces have been tabulated. Similarly, their derivatives were also calculated to ensure the moment produced by them provided optimal control over the aircraft. The dimensions of the various control surfaces are tabulated in Table 7.

TABLE 7
CONTROL SURFACE DIMENSIONS TABLE

Stability Parameter	Parameter	Derivative	Effective Value (per rad)
Aileron (705mm x 52.25mm)	Roll Control Derivative	$C_{L\delta a}$	0.317
Ruddervator (280mm x 71.66mm)	Pitch Control Derivative	$C_{m\delta e}$	-0.33
	Directional Control Derivative	$C_{n\delta r}$	-0.02

IV. POWERPLANT

The propulsion system for vertical take-off and landing is by BLDC motors powered by a Lithium Polymer (LiPo) battery. The optimal thrust to weight ratio for hover is >1.5:1 considering wind gust and other disturbances. The estimated AUW of the UAV is 12000g, so the motor requirements were such that each must produce a thrust of 4500g to obtain decent hover performance. The motor chosen is a KDE 5215XF-435 with 18.5 inch x 6.3 inch propeller producing a thrust of 5040g at 80% throttle. The 4 motors are powered by a 6 cell LiPo battery, the maximum current drawn by the collective motors is about 200 amps.

Fig. 9 KDE 5215XF-435 Motor

Forward flight propulsion is powered by a 2 stroke gasoline engine. The reason to opt for an internal combustion engine as opposed to electric propulsion is that for long endurance missions, an electric motor would need a high capacity battery to power it and the battery would become dead weight when charge is depleted. Whereas an IC engine uses gasoline which is consumed during flight and weight decreases over the course of flight thereby increasing the endurance by a little amount. Another reason to opt for an IC engine is due to the lack of availability of charging stations in remote areas. The engine chosen is a DLE30 2 stroke gasoline engine. The specifics of the engine are given below.

TABLE 8
DLE30 ENGINE SPECIFICATIONS

Parameter	Values
Bore	36mm
Displacement	30.5cc
No. cylinders	1
Fuel Type	Gasoline
Engine Weight	910g
Stroke	30mm

Fig. 10 DLE 30 Engine

Static thrusts conducted on the engine at sea level altitude with 18 inch x 8 inch propeller yielded a thrust of 8500g which conforms to a T/W of 0.7.

V. Autopilot & Mission Planning

The Cube Orange autopilot is the latest and most powerful model in the Cubepilot ecosystem. It is designed for commercial system integrators, UAS manufacturers and hobby users. The Cube Orange autopilot is part of a vast ecosystem of autopilot modules and carrier boards.

Mission Planner is used for configuring the Pixhawk for autonomous missions. The primary goal of the software is to provide control of the aircraft, either autonomously or via pilot input through radio control transmitter or ground control station, or via companion computer onboard the vehicle.

Sensor inputs provide the attitude, position, power system monitoring, and vehicle speed to the autopilot. An I2C based digital airspeed indicator is mounted on the starboard side of the wing. The Cube Orange board has 3 IMUs (accelerometer, gyro, and compass) for redundancy. An external GPS module is used to aid in navigation for auto missions.

VI. Results

A. *CFD Analyses*

CFD Analysis was performed on ANSYS 2020 R1 to study the flow over the aircraft. This study is performed to visualize flow interaction over the aircraft and the data is used to calculate lift and drag. The model was enclosed in a 5m boundary to avoid flow disturbances due to the walls. A grid independent analysis was performed taking element size as the parameter. For each element size, the number of nodes and elements are tabulated as shown in Table 10 with their respective lift and drag values. This study showed us that even with change in mesh parameters, the results stayed constant. The inlet velocity was calculated to be 18 m/s considering the cruise speed. The outlet pressure is set to 0 Pa and no slip wall condition is applied. A K-epsilon turbulence model was chosen due to its good convergence and low memory requirement. The pressure contour and velocity streamlines are obtained for the same. It is inferred from the velocity streamlines that the V Tail is outside the downwash region of the wing. The aircraft produced a lift of 8.8 kg with a drag of 1.2kg. Velocity streamline of the aircraft is shown in Fig. 11, and pressure contour is shown in Fig. 12.

TABLE 9
GRID INDEPENDENT ANALYSIS

Element Size	No of Nodes	Element Size (m)	Lift (N)	Drag (N)
0.1	2387406	13943233	89.78	11.01
0.09	3226549	188883815	89.52	11.08
0.08	4536342	26609088	89.50	11.29
0.07	6701284	39389922	88.92	11.61
0.06	10555983	62183292	88.24	12.08

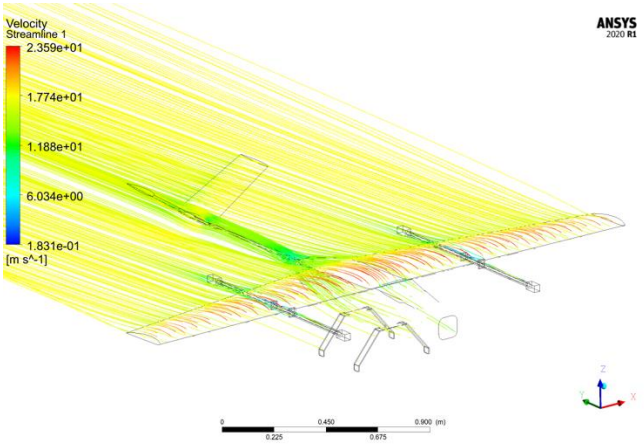

Fig. 11 Velocity Streamline

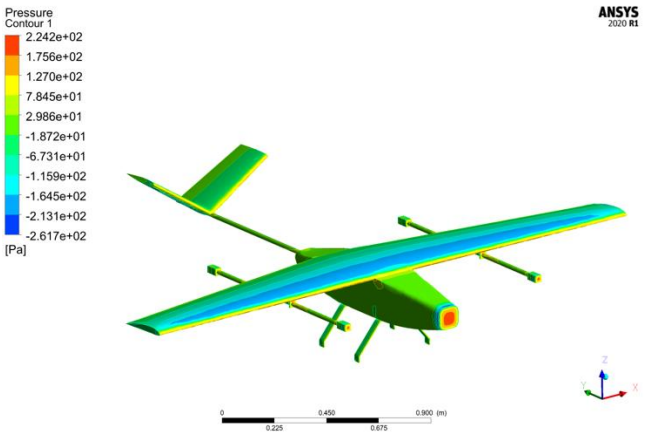

Fig. 12 Pressure Contour

B. STATIC STRUCTURAL ANALYSES

The wing is analysed for deformation under load on Autodesk Fusion 360. The order of the element is chosen to be parabolic with an element size of 0.5 mm for greater accuracy. Proximity and curvature are turned on to achieve greater precision at leading edge, trailing edge and booms where geometry is curved. A Uniformly Distributed Load of 150 N with a factor of safety of 1.5 is applied. The maximum deflection is found to be 0.36 mm and is shown in Fig. 13. The von-Mises stress analysis is also performed to check wing's structural integrity. The maximum von-Mises stress is found to be 21.99 MPa as shown in Fig. 14 which is well below the yield strength of CF which is 3650 MPa. This indicates the wing can handle aerodynamic loads and wing flex during flight. Analysis for the safety factor is shown in Fig. 15.

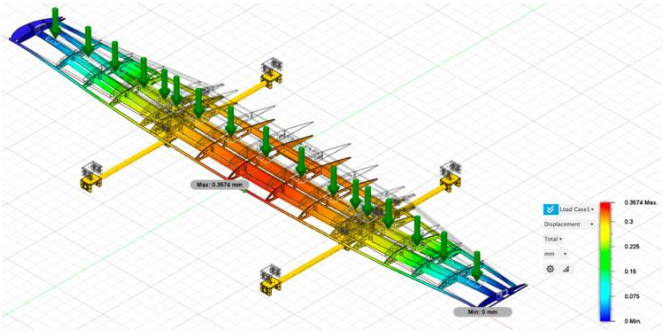

Fig. 13 Displacement under UDL

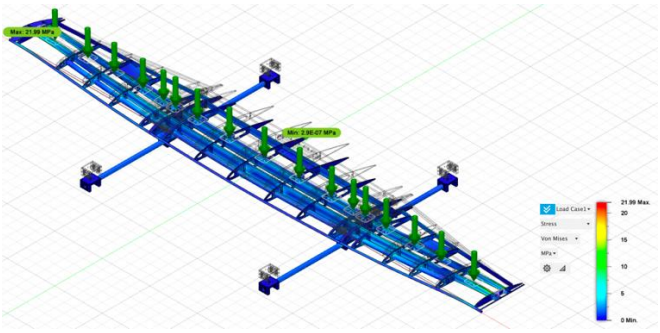

Fig. 14 Von Mises Stress

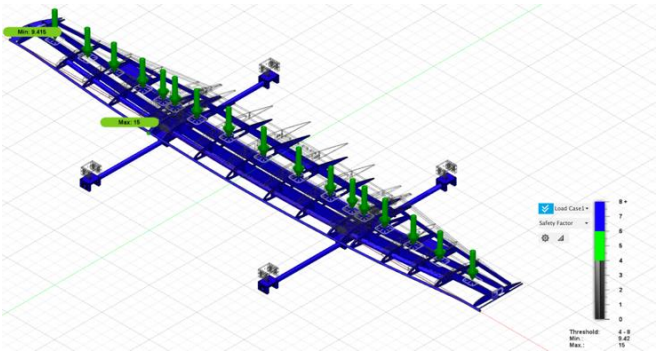

Fig. 15 Safety Factor

C. MODAL ANALYSES

Modal analysis is used to determine the dynamic characteristics of a system. It helps to point out the reasons of vibrations that cause damage to the integrity of system components. Using it, the overall performance of the system in certain operating conditions can be improved. A FEM of the wing has been prepared by modelling the main parts (spars, ribs, VTOL boom) and its modal analysis is carried out on ANSYS 2020 R1. Fluid - structure interaction and inertial load – standard Earth gravity in -Z direction is applied. A fixed-free boundary condition is chosen as it the wing is a cantilever beam resulting in 5 mode shapes. Theoretical approach method is not suitable for aircraft wing due to rigorous and complex

mathematical equations. By modelling current configuration by FEM, it is determined if the current configuration has sufficient strength for loadings. A structurally adequate wing with sufficient stiffness is aimed. The results of the modal analysis carried out are tabulated in Table 10 and images of the same are depicted from Fig. 16 to Fig. 20.

TABLE 10
FREQUENCY RESPONSE OF MODAL ANALYSIS

Mode	Mode 1	Mode 2	Mode 3	Mode 4	Mode 5
Natural Frequency (Hz)	52.957	64.239	91.633	127.04	131.82

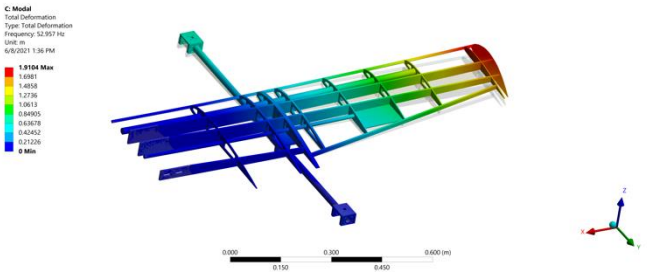

Fig. 16 Mode 1

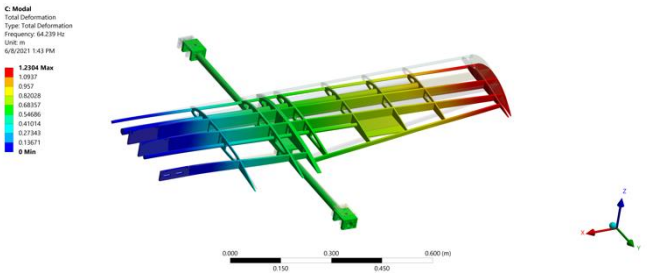

Fig. 17 Mode 2

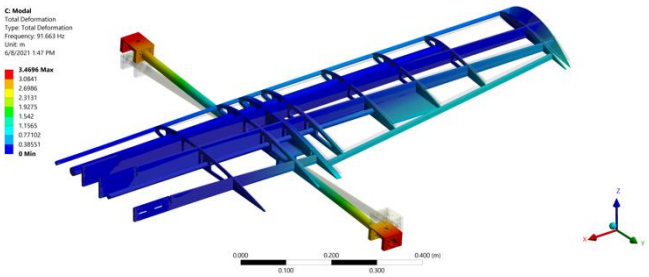

Fig. 18 Mode 3

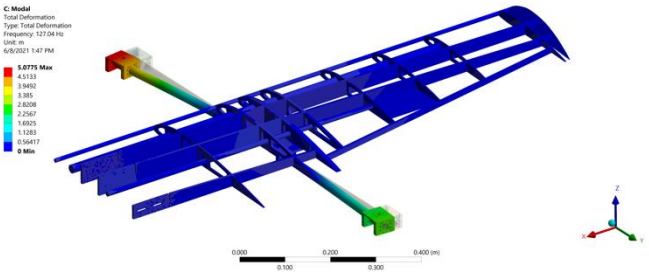

Fig. 19 Mode 4

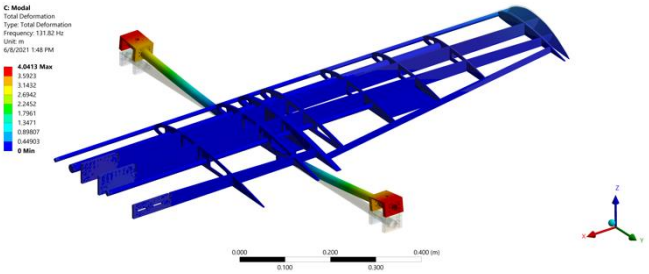

Fig. 20 Mode 5

D. TEST FLIGHTS

Numerous ground checks and system integration checks were performed to test engine tuning, ESC timing, control surfaces and validated the design. Following the ground checks, flights were performed to check takeoff, landing and hover performance. Furthermore, hover tests were done with the engine running to check for vibration impact on autopilot and avionics.

After final tuning and setup, endurance tests were conducted by setting a mission plan consisting of circuits within visual sight by fully auto mission. A 45 minutes endurance was achieved with 1 litre of gasoline fuel.

Fig. 21 Test Flight

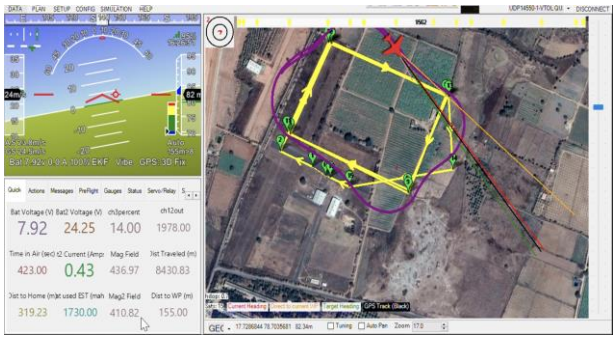

Fig. 22 Mission Planner Screen during Test Flight

VII. CONCLUSION

The designed hybrid VTOL UAV is capable of carrying a payload of 1000 grams with a flight time of 60 minutes. It can take-off and land with a maximum required area of about 25 square meters (that is 5 meter * 5 meter box). It is designed to have adequate structural strength, calculated to optimize flight performance and stability, and analysed to validate the design.

Taking into account of recent event SARS COVID-19, this aircraft is capable of transporting vaccines, medicines to Primary Health Centre and other health care items from distribution location. It utilizes a highly reliable Pixhawk cube-orange autopilot system, which is used to set flight path for autonomous flight plan. Fail safe and return to home option of autopilot makes the aircraft safe and reliable for the purpose of medical cargo delivery within and outside city/town/villages. Rapid transport through highly efficient UAVs holds tremendous potential in this advancing world. The Hybrid VTOL UAV is designed to meet this demand and make the world safer while also improving the facilities in the health department, which is very much essential.

ACKNOWLEDGMENT

We are very grateful to T-Works Foundation, Govt. of Telangana for giving us the unique opportunity to work on the 'VTOL UAV For Medical Cargo Delivery' project. With great pleasure, we extend our gratitude and indebtedness to Department of Aeronautical Engineering of Dayananda Sagar College of Engineering for allowing us to work on the project in collaboration with T-Works Foundation.

REFERENCES

1. *S. M. Metev and V. P. Veiko, Laser Assisted Microtechnology, 2nd ed., R. M. Osgood, Jr., Ed. Berlin, Germany: Springer-Verlag, 1998.*

2. *Breckling, Ed., The Analysis of Directional Time Series: Applications to Wind Speed and Direction, ser. Lecture Notes in Statistics. Berlin, Germany: Springer, 1989, vol. 61.*

3. *S. Zhang, C. Zhu, J. K. O. Sin, and P. K. T. Mok, "A novel ultrathin elevated channel low-temperature poly-Si TFT," IEEE Electron Device Lett., vol. 20, pp. 569–571, Nov. 1999.*

4. *Wegmuller, J. P. von der Weid, P. Oberson, and N. Gisin, "High resolution fiber distributed measurements with coherent OFDR," in Proc. ECOC'00, 2000, paper 11.3.4, p. 109.*

5. *R. E. Sorace, V. S. Reinhardt, and S. A. Vaughn, "High-speed digital-to-RF converter," U.S. Patent 5 668 842, Sept. 16, 1997.*

6. *(2002) The IEEE website. [Online]. Available: http://www.ieee.org/*

7. *M. Shell. (2002) IEEEtran homepage on CTAN. [Online]. Available: http://www.ctan.org/tex-archive/macros/latex/contrib/supported/IEEEtran/*

8. *FLEXChip Signal Processor (MC68175/D), Motorola, 1996."PDCA12-70 data sheet," Opto Speed SA, Mezzovico, Switzerland.*

9. *Karnik, "Performance of TCP congestion control with rate feedback: TCP/ABR and rate adaptive TCP/IP," M. Eng. thesis, Indian Institute of Science, Bangalore, India, Jan. 1999.*

10. *Padhye, V. Firoiu, and D. Towsley, "A stochastic model of TCP Reno congestion avoidance and control," Univ. of Massachusetts, Amherst, MA, CMPSCI Tech. Rep. 99-02, 1999.*

11. *Wireless LAN Medium Access Control (MAC) and Physical Layer (PHY) Specification, IEEE Std. 802.11, 1997.*